International Journal of Control
Vol. 80, No. 11, November 2007, 1701–1716

Taylor & Francis
Taylor & Francis Group

Model predictive control of magnetically actuated mass spring dampers for automotive applications

S. DI CAIRANO†, A. BEMPORAD*†, I. V. KOLMANOVSKY‡ and D. HROVAT‡

†Dipartimento di Ingegneria dell'Informazione, Università di Siena, Italy
‡Ford Motor Company, Dearborn, Michigan, USA

(*Received 10 July 2006; in final form 5 March 2007*)

Mechatronic systems such as those arising in automotive applications are characterized by significant non-linearities, tight performance specifications as well as by state and input constraints which need to be enforced during system operation. This paper takes a view that model predictive control (MPC) and hybrid models can be an attractive and systematic methodology to handle these challenging control problems, even when the underlying process is not hybrid. In addition, the piecewise affine (PWA) explicit form of MPC solutions avoids on-line optimization and can make this approach computationally viable even in situations with rather constrained computational resources. To illustrate the MPC design procedure and the underlying issues, we focus on a specific non-linear process example of a mass spring damper system actuated by an electromagnet. Such a system is one of the most common elements of mechatronic systems in automotive systems, with fuel injectors representing a concrete example. We first consider a linear MPC design for the mechanical part of the system. The approach accounts for all the constraints in the system but one, which is subsequently enforced via a state-dependent saturation element. Second, a hybrid MPC approach for the mechanical subsystem is analysed that can handle all the constraints by design and achieves better performance, at the price of a higher complexity of the controller. Finally, a hybrid MPC design that also takes into account the electrical dynamics of the system is considered.

1. Introduction

During the last few years the major advances in automotive applications have been enabled by "smart" electronic devices that monitor and control the mechanical components. Cars have become complex systems in which electronic and mechanical subsystems are tightly connected and interact to achieve optimal performance. Automotive actuators, in particular, have become mechatronic systems (Barron and Powers 1996, Hrovat *et al.* 2000, Guzzella and Sciarretta 2005) in which mechanical components coexist with electronics and computing devices. These mechatronic automotive systems are characterized by tight operating requirements (such as high precision robustness, low power consumption, fast transition time), significant non-linearities, as well as input and state constraints which need to be enforced during system operation. On the other hand, their dynamics may often be characterized by relatively low-dimensional dynamical models.

Model predictive control (MPC) (Maciejowski 2002, Qin and Badgwell 2003, Camacho and Bordons 2004) is a systematic feedback control design technique which determines the control input via receding horizon optimal control based on an open-loop model of the process, called prediction model. The prediction model is a compromise between simplicity and representativeness of the physics of the process. In particular, complex non-linear systems can be approximated by linear and piecewise linear models whose associated optimal control problem can be solved by relatively

*Corresponding author. Email: bemporad@dii.unisi.it

International Journal of Control
ISSN 0020–7179 print/ISSN 1366–5820 online © 2007 Taylor & Francis
http://www.tandf.co.uk/journals
DOI: 10.1080/00207170701379804

simple numerical procedures. The main appeal of MPC is in being able to enforce pointwise-in-time constraints, while providing the control designer with direct capability to shape the transient response by adjusting the weights in the objective function being minimized. MPC controllers can handle continuous-valued and discrete-valued control inputs, accommodate system parameter changes or subsystem faults, as long as they are reflected in the model used for on-line optimization.

Automotive actuators can often be adequately characterized by low dimensional models, and in this case an explicit implementation of the MPC controller becomes possible (Giorgetti *et al*. 2006a, b), whereby the solution is pre-computed off-line and its representation is stored for on-line application. The on-line optimization is not required and the computational effort can be reduced to the point where the implementation of these control algorithms becomes feasible within the stringent memory and chronometric constraints of automotive microcontrollers.

In this paper we discuss and illustrate an application of MPC-based control design to a magnetically actuated mass-spring-damper system. Such a system consists of a mechanical mass-spring-damper subsystem forced by an electromagnetic subsystem, and it arises very frequently in automotive actuation mechanisms, including fuel injectors (Dyntar and Guzzella 2004) (see also Miller *et al*. (2000), Kolmanovsky and Gilbert (2001) and Isermann (2005) and the references therein). The main control goal is to make the mass position track a given external reference while minimizing the intensity of the control action. The latter tends to lead to a reduction of the energy consumption by the system. Moreover many different constraints must be enforced on both the electromagnetic and the mechanical subsystems. In particular, it is assumed that the electromagnet can only attract but not repel the mass, that the mass is moving within a constrained region, that the mass velocity is bounded, and that the control input is limited.

The force from the coil decays with the square of the distance between the mass and the coil, and is proportional to the square of the electrical current, so that the system is nonlinear and it would require a nonlinear MPC design. By designing an inner-loop controller for the electrical subsystem so that the resulting closed-loop dynamics are sufficiently fast, the overall system is viewed as a constrained second-order linear system (with position and velocity of the moving mass as states) controlled by the magnetic force from the coil.

The paper is organized as follows. The overall model of the magnetically actuated mass-spring-damper system and the operating constraints are introduced in § 2. Due to different time constants of the mechanical and electrical subsystems, a decoupling control approach is presented first in § 3. The approach consists of an MPC controller acting as a reference governor for the electromagnetic system, whose dynamics are regulated by a fast inner-loop controller. In § 4 two MPC designs for the decoupled architecture are presented. The first is based on a linear MPC scheme and it cannot take into account the upper bound on the actual available magnetic force. Such a constraint is enforced by a cascaded saturation block, with a consequent modelling error in the prediction model. The second is a hybrid MPC controller that is also capable of taking into account the constraint on the maximum available force. The decoupled controller architecture and closed-loop experiments are reported in § 5.

In order to assess the limitations introduced by the decoupling assumption of the above designs, where only the mechanical subsystem is optimized by the MPC algorithm, for comparison purposes in § 6 we consider a hybrid MPC controller based on the complete system dynamics. While this approach permits the optimization of the whole system's behaviour, the resulting controller is more complex.

2. Physical model and constraints

The magnetically actuated mass-spring-damper system, whose schematics are shown in figure 1, is a heterogenous system composed by a mechanical subsystem and an electromagnetic subsystem that influence each other. A mass m [kg] moves linearly within a bounded region under the effect of a controlled magnetic force F [N]. Such a force is generated by a coil placed at one of the boundary of the region. Additional forces acting on the mass are generated by a spring and a damper. The overall equations defining the system are

$$m\ddot{x} = F - c\dot{x} - kx, \tag{1a}$$

$$\dot{\lambda} = V - Ri, \tag{1b}$$

$$\lambda = \frac{2k_a i}{k_b + z}, \tag{1c}$$

$$F = \frac{k_a i^2}{(z + k_b)^2} = \frac{\lambda^2}{4k_a}, \tag{1d}$$

$$z = d - x. \tag{1e}$$

Equation (1a) represents the dynamics of the mass position x [m] under the effect of the external force F, of a spring with stiffness k [N/m] and of a damper with coefficient c [N · s/m]. Equation (1b) is Faraday's law for a resistive circuit with resistance R [Ω], subject to magnetic flux variations, where the applied voltage V [V] is the control input. The relation between the magnetic flux λ [V · s] and current i [A] is defined by (1c),

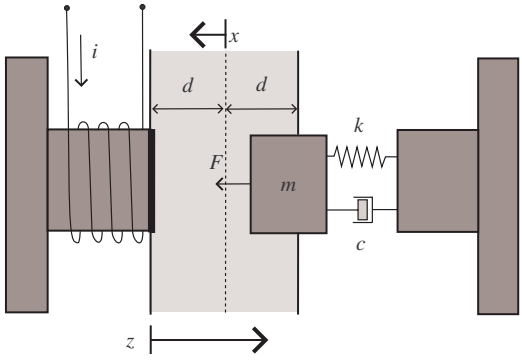

Figure 1. Schematics of a magnetically actuated mass spring damper system.

where k_a, k_b are constants, while equation (1d) defines the magnetic force either as a function of the current or as a function of the magnetic flux. Finally, equation (1e) defines the relation between position coordinates in the mechanical (x) and in the electromagnetic (z) subsystem. The first has the origin at the neutral position of the spring, while the second at the position in which the mass is in contact with the coil. Moreover, since x takes its maximum value at the contact position, and d is the distance between the contact position and the spring neutral position, $z \geq 0$. Note that any bounds on current i immediately become bounds on force F.

The mechanical prediction model considered in this paper takes into account linear spring and viscous friction effects. Additional forces such as stiction or Coulomb friction, that give limited effect since the mass lifts from the coil and only slightly touches it, could have also been included, albeit resulting in a more complex model and higher complexity of the control law. These additional modelling details should be pursued in applications where such effects can significantly degrade the performance of a controller designed on the simplified assumptions, which however is not the case of the application studied in this paper.

The physical model (1) can be expressed as the nonlinear dynamical system

$$\dot{x} = \frac{1}{4k_a m}\lambda^2 - \frac{k}{m}x - \frac{c}{m}d\dot{x}, \tag{2a}$$

$$\dot{\lambda} = -\frac{R(k_b + d)}{2k_a}\lambda + \frac{R}{2k_a}\lambda x + V. \tag{2b}$$

The magnetically actuated mass spring damper is subject to several constraints related to physical limits and performance. The constraint

$$-d \leq x \leq d \quad [\mathrm{m}], \tag{3}$$

where $d = 4 \cdot 10^{-3}$ [m], prevents the moving mass from penetrating the coil or the symmetric stop at the other end, therefore avoiding undesirable bouncing of the moving mass, with consequent noise and increased wear of the parts. Under constraint (3), the simple mechanical model (1a) is valid.

In a number of practical applications for which the problem considered here serves as a prototype, it is actually desirable to control the moving mass so that it is positioned against the coil with $x = d$. In this case, as the moving mass approaches the coil, its velocity needs to be carefully controlled, and the following soft-landing constraint

$$-\varepsilon - \beta(d - x) \leq \dot{x} \leq \varepsilon + \beta(d - x) \quad [\mathrm{m/s}], \tag{4}$$

is imposed, where ε and β are constants. The purpose of soft-landing is to avoid high velocities during collisions (so that noise and wear can be reduced), which also prevents excessive disturbances to the electrical current. When the mass is at the contact position ($x = d$), the velocity is constrained in $[-\varepsilon, \varepsilon]$, a range which is progressively relaxed by β as the mass moves away from the coil. Here we choose ε and β so that for $x = 0$, $\dot{x} \in [-10.2, 10.2]$ m/s, i.e., the constraint is essentially inactive, while for $x = d$, $\dot{x} \in [-0.2, 0.2]$ m/s, i.e., the constraint is quite tight (and difficult to meet). Note that the soft-landing constraint is not required for position $x = -d$ since the moving mass will never be controlled to the symmetric stop, due to the fact that the magnetic force is insufficient to counteract the spring force at $x = -d$.

The current in the circuit cannot be negative and, as a consequence of (1d), the magnetic force is able to only attract the mass

$$i \geq 0 \quad [\mathrm{A}], \tag{5a}$$

$$F \geq 0 \quad [\mathrm{N}]. \tag{5b}$$

In addition, the constraint on the voltage

$$0 \leq V \leq V_{\max} \quad [\mathrm{V}] \tag{6}$$

is enforced to take into account the physical limits and the safety of operation of the electrical circuit.

3. Decoupled control system architecture

Because of the nonlinearity of (2) and of the constraints introduced in the previous section, nontrivial control techniques are required to achieve the required specifications. It is reasonable, however, to assume that the dynamics of the electrical subsystem are much

faster than the mechanical ones. This suggests the possibility of decoupling the control problem, by designing an inner-loop controller acting only on the electrical subsystem, and, under the assumption that the closed-loop electrical dynamics are much faster than the mechanical dynamics, by designing an MPC controller based on the reduced system model

$$\ddot{x} = -\frac{c}{m}\dot{x} - \frac{k}{m}x + \frac{F}{m}, \tag{7}$$

where the position (x) and the velocity ($\dot{x}$) of the mass are the state components and the magnetic force F is the controlled input, subject to constraints (3), (4), (5b) and

$$F \leq k_a \frac{i_{\max}^2}{(d + k_b - x)^2}. \tag{8}$$

Constraint (8) defines an upper bound on the available force, related to the maximum available current $i_{\max}$. Once the force command is computed by the MPC controller, it is passed as a reference to the closed-loop electrical subsystem, which generates the voltage profile required to obtain such a force. The corresponding control system architecture is reported in figure 2, and is structured as follows:

- the MPC controller generates the force profile r_F, based on measurements from the mechanical subsystem (7) and on the reference position r_x for the mass;
- r_F is converted into the current reference profile r_i, which is used as a reference signal by the inner-loop controller regulating the electromagnetic subsystem;
- the inner-loop controller actuates the voltage V to make the current i in the electromagnetic subsystem track r_i;
- the current i generates the actual force F.

In the block diagram depicted in figure 2, the white blocks represent the dynamical subsystems, and the dark-grey blocks represent the controllers. Light-gray blocks represent static blocks: the $r_F \to r_i$ block converts the force reference into the current reference by inverting equation (1d) in the current domain defined by (5a)

$$r_i = \sqrt{r_F \frac{(z + k_b)^2}{k_a}}, \tag{9}$$

the $i \to F$ block represents the transduction (1d) of the current into the magnetic force acting on the mass.

Constraint (8) ensures that the force can be physically generated, given the maximum allowed current $i_{\max}$ in the circuit. The value $i_{\max}$ is computed from (1b) in static conditions, given the maximum voltage $V_{\max}$. Note that (8) defines a non-convex set in the (x, F)-space, being the hypograph of a convex function.

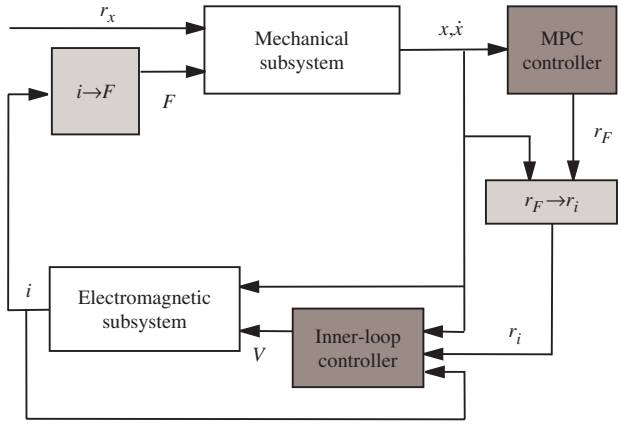

Figure 2. Controller architecture for decoupled MPC design.

3.1 *Inner-loop controller*

The current dynamics defined by (1b) and (1c) are

$$\frac{\mathrm{d}i}{\mathrm{d}t} = \frac{k_b + z}{2k_a} V - \frac{k_b + z}{2k_a} Ri + \frac{1}{k_b + z} i \frac{\mathrm{d}z}{\mathrm{d}t}. \tag{10}$$

A way to make the current i track the desired reference r_i given the non-linear dynamics (10) is to design a controller $V = g(i, z, \mathrm{d}z/\mathrm{d}t, r_i)$ by feedback linearization. By letting $di/dt = f(i, z, \mathrm{d}z/\mathrm{d}t, V)$ be dynamics (10), the control law

$$V = \frac{2k_a}{k_b + z}\left(\frac{k_b + z}{2k_a} Ri - \frac{1}{k_b + z} i \frac{\mathrm{d}z}{\mathrm{d}t} - \beta i + \gamma r_i\right), \tag{11}$$

is chosen by imposing that $\mathrm{d}i/\mathrm{d}t = f(i, z, \mathrm{d}z/\mathrm{d}t, g(i, z, \mathrm{d}z/\mathrm{d}t, r_i)) = -\beta i + \gamma r_i$, with $\beta, \gamma > 0$, so that the closed-loop current dynamics become linear first-order dynamics with a stable pole $p_i = -\beta$ and steady-state gain γ/β.

In the decoupled MPC design approach the behaviour of the whole system largely depends on the dynamics imposed by the feedback linearization controller for the electromagnetic subsystem. In particular, mass position and velocity are treated as disturbances acting on the electromagnetic subsystem, and should be slowly varying with respect to the electromagnetic variables.

Drawbacks of the proposed feedback linearization controller are that the voltage command can take large values and vary rapidly, that the controller requires

also the velocities to be estimated, while often the only position is measured in such actuators, and that small modelling errors can cause loss of stability or performance degradation. Since the main concerns here are the properties of the decoupled MPC design, for simplicity we proceed with the assumption that the inner-loop controller is the feedback linearization controller (11), while noting that a more robust design, for instance based on backstepping techniques, could be used as an alternative.

3.2 *Model predictive controller*

The overall idea behind the decoupled design is to exploit a nonlinear controller to obtain a linearization of the dynamics, and to use a model predictive controller to meet specifications and performance. Because of the short sampling period required by automotive actuators, standard non-linear MPC techniques based on smooth nonlinear optimization to be solved in real-time (Rawlings 2000) are not applicable in the present context. Hence, linear and hybrid MPC controllers that can be implemented in an explicit form (Bemporad *et al*. 2002) are considered here. Other techniques that may be applicable include suboptimal explicit non-linear MPC (Johansen 2004) and implicit MPC implemented on appropriate hardware architectures (Bleris *et al*. 2006, Ling *et al*. 2006). However, the evaluation of such recent techniques is out of the scope of this paper, and it may be the subject for future investigations.

In the next section we propose two MPC schemes based on linear and hybrid prediction models, respectively.

4. Linear and hybrid decoupled model predictive control

Conventional linear feedback controllers, such as LQR controllers, do not explicitly handle pointwise-in-time constraints on system's inputs, states, and outputs. On the other hand, model predictive control is an optimization-based closed-loop control strategy in which such constraints can be explicitly embedded into the controller (Rawlings 2000, Maciejowski 2002, Qin and Badgwell 2003).

We consider two different types of MPC controllers for the decoupled architecture proposed in the previous section: (1) a linear model predictive controller obtained by neglecting the non-linear constraint (8), which is enforced later by a state-dependent saturation function, and (2) a hybrid model predictive control law which considers a piecewise affine approximation of (8).

As observed earlier, in the MPC design we assume that the dynamics of the electrical subsystem in closed-loop with the inner-loop controller are infinitely fast, that is $F = r_F$. Thus, with a slight abuse of notation, we will refer to F as the output of the MPC controller. The effects of the electrical dynamics will be analysed in § 5.

4.1 *Decoupled linear model predictive control*

As MPC requires a discrete-time model, the mechanical dynamics (7) are discretized in time with sampling period $T_s = 5 \cdot 10^{-4}$ [s]

$$\xi(k+1) = A\xi(k) + Bu(k), \tag{12}$$

where

$$\xi = \begin{bmatrix} x \\ \dot{x} \end{bmatrix}, \quad u = F.$$

In addition, the output-equation $y(k) = C\xi(k)$, where

$$y = \begin{bmatrix} x \\ \dot{x} + \beta x \\ \dot{x} - \beta x \end{bmatrix},$$

is introduced to specify the desired performance and for imposing constraints on velocity.

The MPC strategy is based on the solution of the optimal control problem

$$\left.\begin{aligned} \min_{\{\Delta u_k\}_{k=0}^{N_U-1}} & \sum_{k=0}^{N_J-1} (x_{k+1} - r_x(t))' Q_x (x_{k+1} - r_x(t)) \\ & + \Delta u_k' Q_{\Delta u} \Delta u_k + \rho\sigma^2 \\ \text{subject to } & y_{\min} - \sigma\mathbf{1} \le y_k \le y_{\max} + \sigma\mathbf{1}, \quad k = 1, \ldots, N_C \\ & u_{\min} \le u_k \le u_{\max}, \quad k = 0, \ldots, N_U - 1 \\ & \Delta u_{\min} \le \Delta u_k \le \Delta u_{\max}, \quad k = 0, \ldots, N_U - 1 \\ & \Delta u_k = 0, \quad k \ge N_U \\ & \xi_{k+1} = A\xi_k + Bu_k \\ & y_k = C\xi_k + Du_k, \; x_k = [1\ 0]\xi_k, \\ & k = 0, \ldots, N_J - 1 \\ & \sigma \ge 0, \end{aligned}\right\} \tag{13}$$

where $\Delta u_k = u_k - u_{k-1}$, and $u_{-1} = u(t-1)$ is the previous input. N_J is the prediction horizon used to define the performance index, $N_C \le N_J$ is the horizon along which the output constraints are enforced, and N_U is the number of free control actions, $N_U \le N_J$ and $u_k = u_{N_U-1}$, $\forall k = N_U, \ldots, N_J$. The slack variable σ (also called "panic variable") is introduced to soften output constraints (vector $\mathbf{1}$ has all its entries equal

to one), therefore preventing infeasibility and a consequent halt of the control algorithm (the weight ρ is significantly higher than the other weights in the objective function). If $\rho = \infty$, hard constraints are enforced ($\sigma = 0$).

The MPC algorithm can be summarized as follows. At each sampling instant t

1. set

$$\xi_0 = \begin{bmatrix} x(t) \\ \dot{x}(t) \end{bmatrix};$$

2. solve problem (13) obtaining the optimal inputs $u_0^*, \ldots, u_{N_U-1}^*$;
3. use $F(t) = u_0^*$ as the reference force for the inner-loop controller and discard the remaining optimal inputs.

The complexity of the MPC algorithm clearly depends on the structure of the optimization problem. In particular, as the system dynamics and the design constraints are linear and problem (13) involves only continuous-valued variables, the MPC algorithm requires, at each time step t, the solution of a quadratic program (QP), for which solution algorithms of polynomial complexity exist (Boyd and Vandenberghe 2004).

Constraint (8), which is disregarded in (13), is enforced *a posteriori* by the saturation function

$$\tilde{u} = \begin{cases} u_0^* & \text{if} \quad u_0^* \le k_a \dfrac{i_{\max}^2}{(d + k_b - x)^2} \\ k_a \dfrac{i_{\max}^2}{(d + k_b - x)^2} & \text{if} \quad u_0^* > k_a \dfrac{i_{\max}^2}{(d + k_b - x)^2}. \end{cases} \tag{14}$$

If constraint (8) is rarely active, the resulting MPC controller cascaded by the state-dependent input-saturation may be sufficient for adequately controlling the system, and simple and relatively easy to compute at the same time. On the other hand, if constraint (8) is often active, the predicted trajectory will largely differ from the actual one, because of the unmodelled state-dependent input saturation (14). In the latter case, the system performance will most likely be degraded.

For the magnetically actuated mass spring damper, the linear-MPC controller was designed using the Hybrid Toolbox (Bemporad 2003), with

$$y(t) = \begin{bmatrix} 1 & 0 \\ 2500 & 1 \\ -2500 & 1 \end{bmatrix} x(t) \tag{15}$$

and

$$Q_x = 10^4, \quad Q_u = 10^{-10}, \quad \rho = \infty$$

$$y_{\min} = \begin{bmatrix} -4 \cdot 10^{-3} \\ -\infty \\ -10.2 \end{bmatrix}, \quad y_{\max} = \begin{bmatrix} 4 \cdot 10^{-3} \\ 10.2 \\ +\infty \end{bmatrix},$$

$$u_{\min} = 0, \quad u_{\max} = 10^4, \quad -\Delta u_{\min} = \Delta u_{\max} = \infty,$$

$$N_J = 30, \quad N_C = 5, \quad N_U = 3.$$

Figure 3 shows the behaviour of nominal (ideal) closed-loop formed by the linear model and the MPC controller when tracking a desired reference profile,

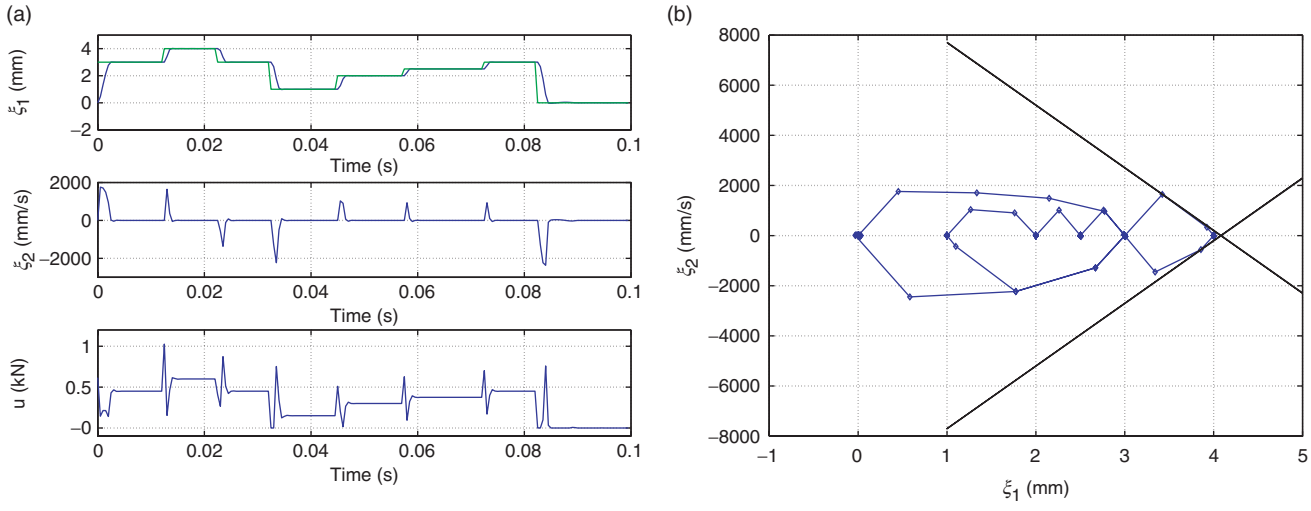

Figure 3. Linear closed-loop MPC simulation (ideal case of no position-dependent force constraints and of infinitely fast electrical dynamics): (a) state and input trajectories; (b) phase-plane trajectories.

over a simulation time interval of 0.1 seconds from the initial state

$$\xi(0) = \begin{bmatrix} 0 \\ 0 \end{bmatrix}.$$

The corresponding position, velocity and input profiles are reported in figure 3(a), while the phase plane in which satisfaction of velocity constraint (4) is shown in figure 3(b). This velocity constraint only becomes active near the contact position $x = d$. Because the controller cannot provide quick decelerations due to the unidirectionality of the magnetic force, constraint (4) is kept inactive by the MPC controller when away from the contact point.

Figure 4(a) shows that the simplification introduced by removing constraint (8) is actually unjustified. In figure 4(a), the curved line representing the upper bound on the force of equation (8) as a function of the moving mass position $x = \xi_1$ is superimposed on the input signal generated by MPC, showing that constraint (8) is often violated. The effects of such a simplification after the variation of the set-point in the negative direction are apparent in figure 4(b), which shows the behaviour of the closed-loop system when the position-dependent saturation block (14), enforcing constraint (8), is cascaded to the MPC controller.

The reason for the degradation of the tracking performance is that the linear MPC controller is not aware that braking the mass at large distances away from the coil is impossible because of the state-dependent input saturation. This is in fact seen from the input plot in figure 4(b) where the dashed line corresponds to the output of the MPC controller, while the solid line corresponds to the output of the saturator.

To avoid wide oscillations and long settling periods, the saturation constraint (8) should be taken into account in the MPC setup. Unfortunately, (8) is a non-convex constraint that cannot be handled by standard linear MPC. Next section shows how such a constraint can be handled by a hybrid MPC approach.

4.2 *Decoupled hybrid model predictive control*

The general idea of the approach is to approximate non-linear dynamics and constraints through piecewise affine functions (referred to as "hybridization" process) and to formulate the optimization problem on the approximated model, which has the form of a piecewise affine (PWA) system (Sontag 1981). PWA systems can be recast as mixed logical dynamical (MLD) systems (Bemporad and Morari 1999), a more convenient prediction model whose associated optimal control problem can be solved by mixed-integer programming.

The resulting hybrid MPC controller usually performs satisfactorily in terms of both tracking performance and constraint handling, even if the hybrid prediction model is only an approximation of the real system.

The hybrid MPC approach can be summarized as follows: first, the non-linear dynamics and constraints are approximated by a piecewise affine function; second, the resulting piecewise affine system is modeled as an MLD system; finally, the MLD system is used as a prediction model in the MPC algorithm. The above steps are detailed here below for the problem tackled in this paper.

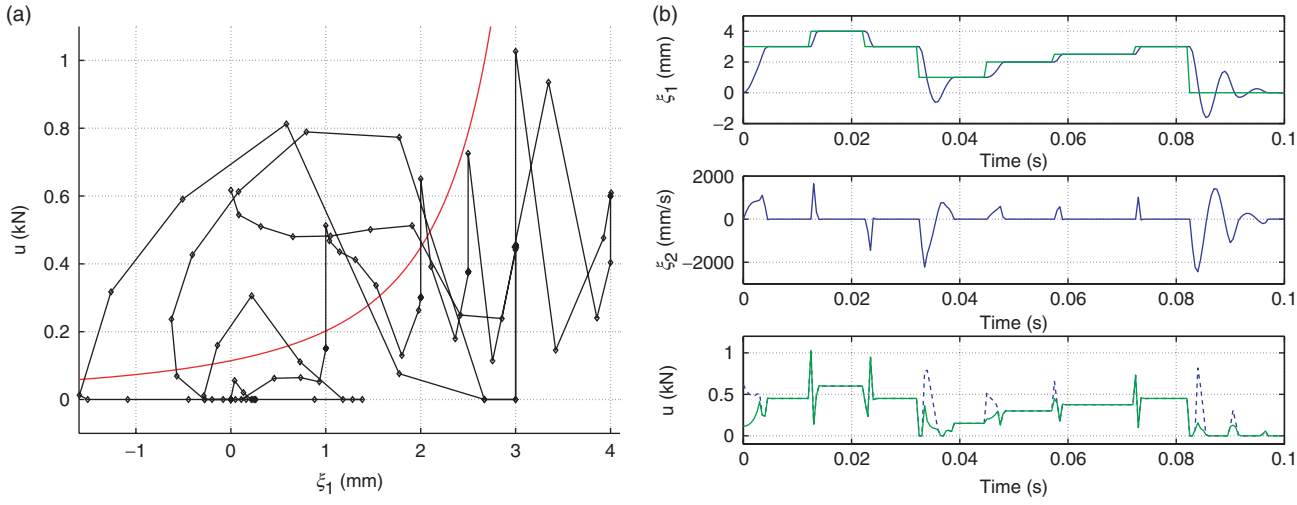

Figure 4. Effects the saturation (14) cascading linear MPC controller: (a) input value generated by the linear MPC controller vs. position and curve representing the position-dependent upper-bound of the available current; (b) state and input trajectories when (8) is enforced *a posteriori*. The superimposed dashed line in the bottom figure is the non-saturated input.

1. Hybridization of non-linear functions. We consider here the simple case of hybridization of a (possibly discontinuous) one-dimensional function into the piecewise affine form $f(\chi) = r_i\chi + q_i$, if $\chi \in [\bar{\chi}_i, \bar{\chi}_{i+1})$, $i = 0 \dots \ell - 1$, where $\bar{\chi}_i < \bar{\chi}_{i+1}$. The points $\{\bar{\chi}_i\}_{i=1}^{\ell-1}$ are the function breakpoints and define the borders between regions in which $f(\chi)$ has different affine terms. Next, we introduce $\ell - 1$ binary variables $\delta_1, \dots \delta_{\ell-1} \in \{0, 1\}$ defined by the logical conditions

$$[\delta_i = 1] \leftrightarrow [\chi \leq \bar{\chi}_i], \quad i = 1, \dots, \ell - 1, \tag{16}$$

and $\ell - 1$ continuous variables $z_1, \dots, z_{\ell-1} \in \mathbb{R}$ defined by

$$z_i = \begin{cases} (r_{i-1} - r_i)\chi + (q_{i-1} - q_i) & \text{if } \delta_i = 1 \\ 0 & \text{otherwise} \end{cases} \quad i = 1, \dots \ell - 2, \tag{17a}$$

$$z_{\ell-1} = \begin{cases} r_{\ell-2}\chi + q_{\ell-2} & \text{if } \Delta_\ell - 1 = 1 \\ r_{\ell-1}\chi + q_{\ell-1} & \text{otherwise.} \end{cases} \tag{17b}$$

Then, the piecewise affine approximation is

$$f(\chi) = \sum_{i=1}^{\ell-1} z_i. \tag{18}$$

Relations (16), (17), (18) can be embedded into an MLD system, using for instance the modelling language HYSDEL (Torrisi and Bemporad 2004), along with the logical constraints

$$[\delta_i = 1] \rightarrow [\delta_{i+1} = 1], \quad \forall i = 1, \dots, \ell_i \tag{19}$$

which are included to largely simplify the complexity of the MPC optimization problem associated with the MLD model.

The non-linear and non-convex force constraint (8) is approximated by a piecewise affine approximation with three segments ($\ell = 3$), and as a consequence, two δ and two z auxiliary variables have been introduced. The force constraint (8) is defined as

$$u \leq z_1 + z_2, \tag{20}$$

where z_1 and z_2 are defined by (16) and (17) with $\chi = x$ and $\ell = 3$. Clearly $f(x) = z_1 + z_2$ is the function that approximates the right-hand side of (8).

2. Hybrid MPC design. Model (7) with (15), (16), (17), (20), can be modelled in HYSDEL (Torrisi and Bemporad 2004), and the equivalent Mixed Logical Dynamical (MLD) hybrid model (Bemporad and Morari 1999)

$$\xi(k+1) = A\xi(k) + B_1 u(k) + B_2\delta(k) + B_3 z(k), \tag{21a}$$

$$y(k) = C\xi(k) + D_1 u(k) + D_2\delta(k) + D_3 z(k), \tag{21b}$$

$$E_2\delta(k) + E_3 z(k) \leq E_1 u(k) + E_4\xi(k) + E_5, \tag{21c}$$

corresponding to the saturated magnetic actuator is obtained, where the matrices A, B_i, $i = 1 \dots 3$, E_j, $j = 1, \dots 5$, are generated automatically in MATLAB using the Hybrid Toolbox (Bemporad 2003).

The hybrid MPC optimization problem is formulated as

$$\min_{\{u_k\}_{k=0}^{N-1}} (\xi_N - r_\xi)^T Q_N (\xi_N - r_\xi) + \sum_{k=0}^{N-1} (\xi_k - r_\xi)^T Q_\xi (\xi_k - r_\xi) + u_k Q_u u_k + \rho\sigma^2 \tag{22a}$$

subject to MLD dynamics (21), (22b)

$$y_{\min} - \sigma\mathbf{1} \leq y_k \leq y_{\max} + \sigma\mathbf{1}, \quad k = 1, \dots, N, \tag{22c}$$

$$u_{\min} \leq u_k \leq u_{\max}, \quad k = 0, \dots, N-1, \tag{22d}$$

$$\sigma \geq 0, \tag{22e}$$

where (22c) models (3) and (4), and (22d) models (5b). Here, we choose

$$Q_\xi = Q_N = \begin{bmatrix} 2 \cdot 10^6 & 0 \\ 0 & 0 \end{bmatrix},$$

$Q_u = 10^{-7}$, $N = 3$, $\rho = \infty$. Output constraints, where $y_{\min}$ and $y_{\max}$ are the same as for problem (13), may be enforced as soft constraints, while input constraints, where $u_{\min} = 0$ and $u_{\max} = +\infty$, and the approximation of (8), which is embedded into the MLD model, are always enforced as hard constraints.

Because of the binary variables δ, the hybrid MPC strategy (22) requires the solution of a mixed-integer quadratic program. Here only two binary variables are considered for each prediction step, so that for short prediction horizons the resulting optimization problem is of very small size.

The resulting closed-loop trajectories of the simulation scenario proposed in § 4.1 when the hybrid MPC control algorithm is applied are reported in figure 5. Note that the piecewise affine approximation (16), (17) is a lower bound to the maximum force, so that the force generated by the hybrid MPC algorithm never exceeds the saturation limits. With respect to the simulation of the linear MPC cascaded by the saturation block (reported as dashed line in the position trajectory plot in figure 5) the system reacts slightly slower when starting from the neutral position $\xi(0) = [0\ 0]'$. This is the effect of the

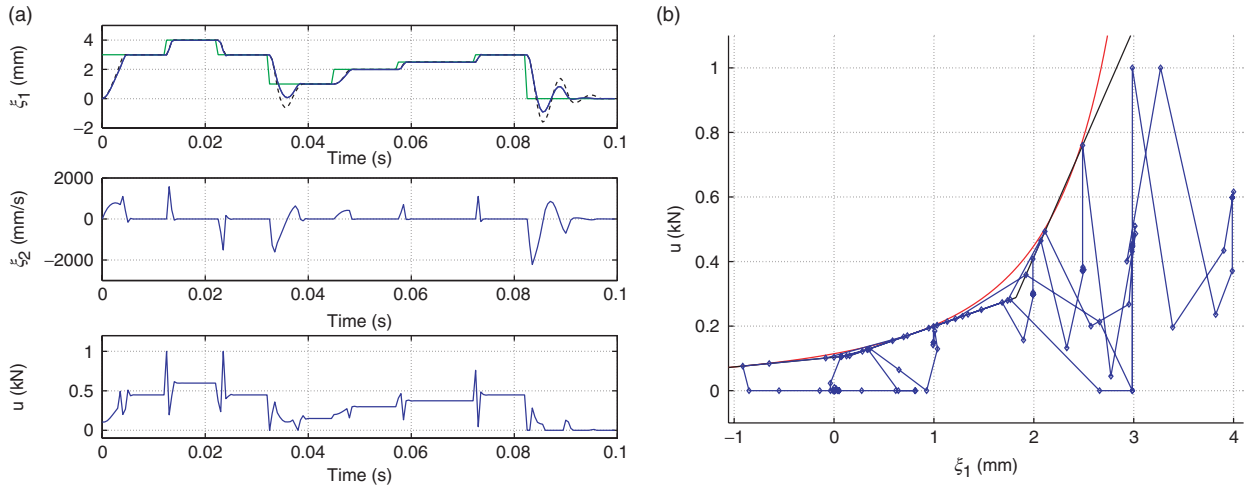

Figure 5. Closed-loop simulation using the hybrid MPC controller (22): (a) State and input trajectories: the superimposed dashed line in the top figure is the position trajectory obtained with saturated linear MPC; (b) nonlinear force constraint, its PWL approximation, and input values generated by hybrid MPC.

conservative approximation of the force constraint. While such a negative effect could be eliminated by introducing a more refined approximation, the positive effects of the hybrid MPC controller are clear when the reference decreases. Both the undershoot and the settling period are reduced, because the controller is now aware of the available magnetic force. Soft-landing constraints are fully satisfied similarly to what was reported in figure 3(b).

Table 1 compares the cumulated squared position errors $\sum_k (x(k) - r_x(k))^2$ and cumulated squared inputs $\sum_k u(k)^2$ for the different MPC control scenarios. The tracking performance is clearly worse than in the ideal linear MPC scenario (no force saturation), but the hybrid controller provides better performance (around 15%) with respect to saturated linear MPC. Note also that a certain component of the tracking error is intrinsically due in all cases by the one-step delay in reacting to reference changes, due to the non-anticipative implementation of the MPC algorithms. Such an error, that with respect to data in table 1 has a value of 25.5, is independent of the controller applied, and thus should not be considered in comparing performances. Following this reasoning, the increase of net performance of the hybrid MPC algorithm is about 20% with respect to the linear-saturated one.

5. Explicit MPC, implementation issues, and simulation results

We consider important implementation issues of the aforementioned control schemes on hardware. First we derive an equivalent piecewise affine form of the control laws, and then analyse the effects of the dynamics of the electrical current under the controller based on feedback linearization.

Table 1. Comparison of the three MPC scenarios.

MPC controller	Cumulated position error (mm^2)	Cumulated square inputs (kN^2)
Linear (ideal)	51.4679	29.1918
Linear saturated	97.8608	26.6314
Hybrid	83.1005	26.6588

5.1 *Explicit implementation of the controller*

The implementation of the MPC controllers described in §4 in an automotive microcontroller may be prevented by the excessive time required for the on-line solution of the MPC optimization, given the very short sampling time $T_s = 0.5$ ms. In Bemporad *et al.* (2002) it is shown that the solution to problem (13) can be obtained as a function of the parameters ξ_0 and r_x (i.e., the actual position, velocity and position reference) by using multiparametric quadratic programming (mp-QP). Using the mp-QP solver in the Hybrid Toolbox, we obtain an explicit feedback law $u(\xi, r_x)$ in continuous piecewise affine form consisting of 80 regions, which can be evaluated on-line very quickly, as the largest part of the computations have been performed off-line by the mp-QP solver. The mp-QP algorithm also returns the value function $\mathcal{V}(\xi, r_x)$, which is a convex piecewise quadratic function. It must be stressed that the implicit MPC controller and the explicit one produce the same results, but there is a difference in the amount of computation

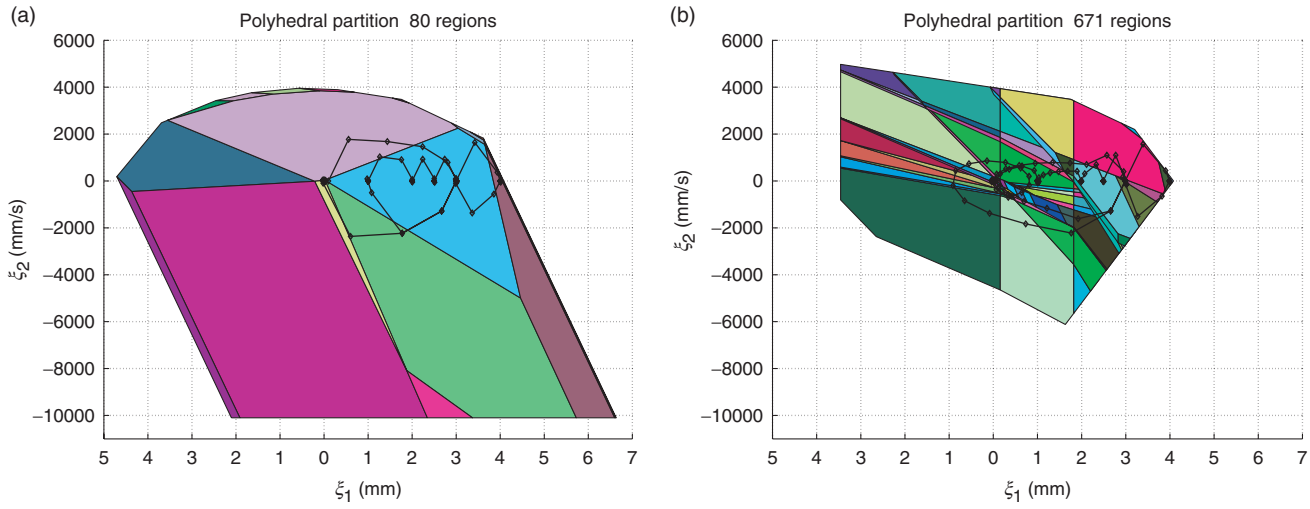

Figure 6. Section of the explicit controller partitions obtained for $r_x = 0$: (a) Linear explicit MPC controller; (b) Hybrid explicit MPC controller.

required at each sampling step. More specifically, this difference is between the solution of an online optimization problem versus the evaluation of a set of inequalities and the computation of an affine state feedback term.

Figure 6(a) shows a section of the three-dimensional polyhedral partition of the explicit linear MPC controller (where hard input/state/output constraints are enforced, i.e., $\rho = \infty$) obtained for $r_x = 0$. There is an affine state feedback controller associated to each region in the partition. Figure 6(a) also shows the state trajectory superimposed over the polyhedral partition.

In the case of hybrid MPC, we use the algorithm of Bemporad (2003) to obtain a representation of the MPC controller as a set of (possibly overlapping) continuous piecewise affine controllers. During on-line operation, the corresponding value functions $\mathcal{V}$ are evaluated and compared to determine the command input with minimum cost. Thus the explicit hybrid MPC solution involves the potential additional operation of comparing the value functions on-line. In our case, the number of regions increases to 671, thus the controller requires a larger storage memory in the microcontroller and a certain (typically small) number of comparisons to find the active controller region.

5.2 *Simulation of the decoupled MPC architecture*

We analyse now the effect of the neglected dynamics of the electrical current. We have tested the decoupled linear/hybrid MPC approach and compared the results with the ones obtained in the ideal case, in which the dynamics of the electromagnetic subsystem are infinitely fast.

The inner-loop controller (11) is designed with $\beta = \gamma = 1.5 \cdot 10^5$. Since the mechanical subsystem is a second-order under-damped system with damped frequency peak at $\omega_r = 950\,\text{rad/s}$ and -3db bandwidth $BW_3 = 3 \cdot 10^3\,\text{rad/s}$, the feedback linearization controller imposes a current dynamics ($BW_3 = 1.5 \cdot 10^5\,\text{rad/s}$) which is much faster than the mechanical one.

We consider a square wave between the critical value 4 mm and 0 mm and with frequency 15 Hz as the position reference r_x. The initial state is $\xi_0 = [0\ 0]^T$.

Figure 7 reports the results obtained with the linear MPC controller (13) cascaded by the saturator (14), where the inner-loop controller is (11). In figure 7(a) the position of the mass (solid) and its reference (dashed) are shown. Figure 7(b) reports the difference $d_x(t) = x(t) - x^{(MPC)}(t)$, where x is the position obtained by the decoupled linear MPC, in which the current dynamics are imposed by the feedback linearization controller, while $x^{(MPC)}$ is the nominal linear MPC position + saturation but assuming infinitely fast current dynamics. The difference is rather small (in the order of tens of micrometers), because of the fast response of the controlled current dynamics. Note that the position constraints are slightly violated, mainly because of the neglected current dynamics, but only for a limited amount. Thanks to the use of soft constraints, the MPC algorithm always returns a control action.

Figure 8 reports the situation in which the hybrid MPC (22) is used with (11) as an inner-loop controller. Figure 8(a) reports the position of the mass (solid) and its reference (dashed), and figure 8(b) reports the difference $d_x(t)$ between position of the decoupled hybrid MPC and of the nominal MPC. It is evident that the hybrid MPC controller is better than the

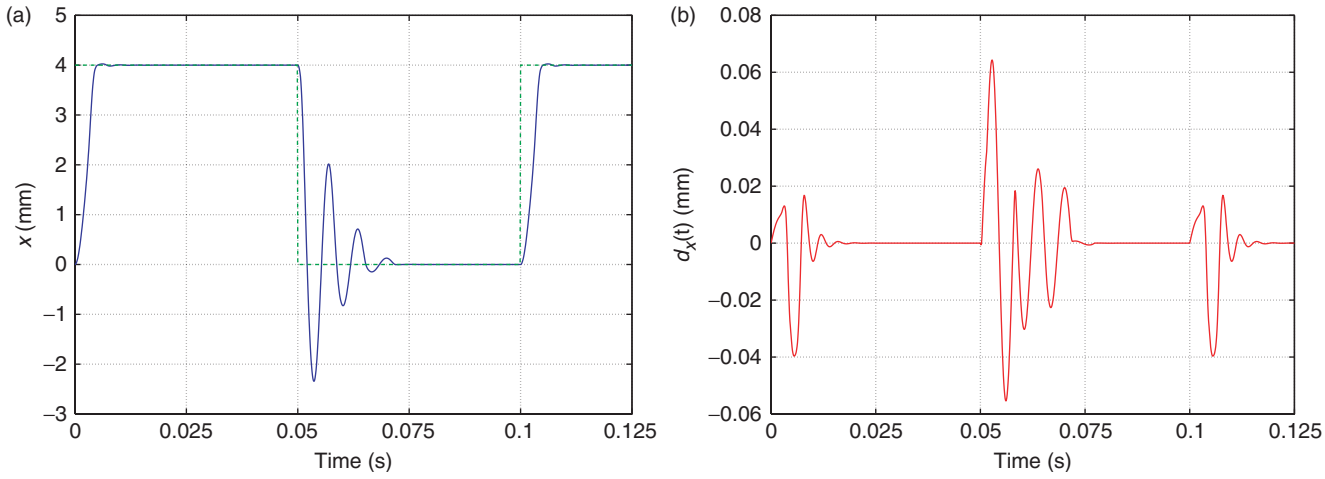

Figure 7. Decoupled linear MPC of the mass-spring-damper system: (a) tracking performance; (b) position difference $d_x(t)$ between the decoupled linear MPC and the nominal MPC.

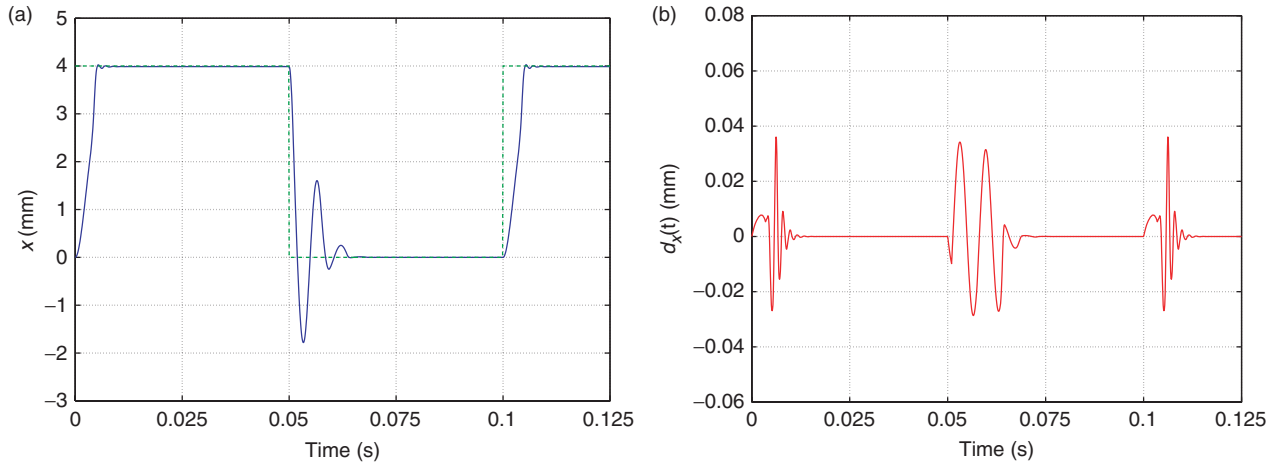

Figure 8. Decoupled hybrid MPC of the mass-spring-damper system: (a) tracking performance; (b) position difference $d_x(t)$ between the decoupled hybrid MPC and the nominal MPC.

linear one in both the difference $d_x(t)$, which is almost halved, and in tracking performance, especially in the transition from 4 mm to 0 mm. The increase of performance is paid by a higher complexity of the controller, since the hybrid MPC algorithm requires at each step the solution of a mixed-integer program instead of the convex quadratic program of linear MPC. In terms of CPU time, for simulating the closed-loop system (system's dynamics, feedback linearization controller, and MPC controller) in Simulink over 0.125 s (=250 sampling steps) a Pentium-M 2 GHz computer with 1 GB RAM running Cplex 9.1, Matlab 7 and the Hybrid Toolbox takes 4 s to simulate the decoupled linear implicit MPC controller, and 6.5 s for the decoupled hybrid implicit MPC. When the the nonlinear system is in closed loop with the explicit linear MPC and the feedback linearization controllers the simulation time is 1.54 s; if the explicit hybrid MPC is used instead, the time is 0.89 s. To evaluate the computation time required by the explicit MPC controllers we have randomly generated 100 points in the controller partitions, and we have evaluated the CPU time in the C code automatically generated by the Hybrid Toolbox on the same computer used for simulation. The average and the worst-case CPU time for evaluating the control input are reported in table 2 for the linear and hybrid controllers, together with the corresponding data-memory occupancies. Even if the controller is not executed on a dedicated hardware, the computation time is shorter than the sampling period also in the

worst case. This suggests that if the C code is optimized and executed on a dedicated hardware, e.g., on a FPGA device, the CPU time would be significantly smaller than the sampling period.

The worst-case number of operations that the controller has to perform in a sampling unit are reported in table 3. Such worst case is almost exceptional and for the explicit hybrid MPC the reported numbers are also upper bounds. According to such data and not accounting for the inner loop current controller, a device that executes one operation per clock period and runs at about 200 MHz seems suitable for implementation of both MPC controllers even in the most pessimistic situation.

We finally show that in case slower dynamics of the current are imposed by the feedback linearization controller, the performance clearly degrades. Figure 9 shows the results for the linear decoupled MPC that tracks a square reference with frequency 15 Hz, higher value 3.1 mm and lower value 0 mm. In this case the feedback linearization controller parameters are $\beta = \gamma = 5 \cdot 10^3$, and the closed-loop current dynamics have bandwidth $BW_3 = 5 \cdot 10^3$ rad/s, the same order of magnitude as the one of the mechanical subsystem. The tracking performance is largely degraded and the difference between the decoupled MPC and the nominal MPC trajectory is increased by an order of magnitude. When the reference has larger amplitude or the imposed current dynamics are slower, larger constraint violations and numerical instability of the MPC algorithm also occur.

The feedback linearization controller is not designed to enforce voltage constraints. The voltage could be limited by inserting a saturation block between the feedback linearization controller and the electromagnetic subsystem, at the price of a possible reduction of the overall tracking performance. In the next section, we explicitly take into account voltage constraints in the design by considering a hybrid prediction model of the full system.

Table 2. CPU time and data memory occupancy for the explicit linear and hybrid controllers.

Explicit controller	Average CPU time	Worst-case CPU time	Data memory
Linear MPC	0.005 ms	0.2 ms	17 KB
Hybrid MPC	0.025 ms	0.3 ms	98 KB

Table 3. Worst case number of operations to be executed in a sampling unit.

Explicit controller	# multiplications	# sums	# comparisons
Linear MPC	3689	3163	526
Hybrid MPC	12609	8700	3930

6. Coupled model predictive control

The decoupled MPC has been proven to be feasible even by using a simple feedback linearization controller as an inner-loop controller. However, in this approach the MPC algorithm does not take into account the current dynamics and, as a consequence, it cannot optimize the behaviour of the entire system and enforce voltage constraints.

In order to analyse the degree of optimality of the decoupled MPC approach we can design an MPC

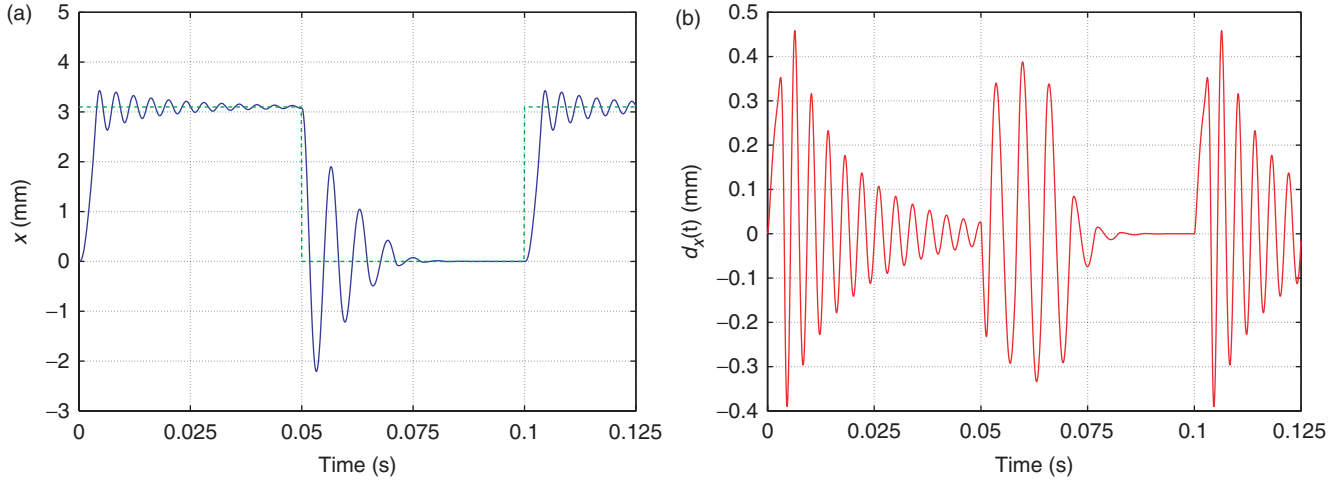

Figure 9. Performance degradation caused by slow current dynamics: (a) tracking performance; (b) position difference $d_x(t)$ between the decoupled linear MPC and the nominal MPC.

controller which takes into account both the mechanical and the electromagnetic subsystems. The control loop becomes a standard feedback loop, in which the MPC receives the reference and the measurements of both the mechanical and electromagnetic states, and chooses the voltage to be applied to the system for optimizing the performance, while satisfying all the constraints.

6.1 *Model of the overall system*

The non-linear dynamics (2) cannot be used as a prediction model for linear/hybrid MPC, since it cannot be embedded into a quadratic optimization problem with integer variables. However, we can apply again the approach of § 4.2.1 to find a piecewise affine approximation of (2).

To this end consider (2b) and the following change of variable, $\Lambda = \ln(\lambda/\lambda_0)$, where $\lambda_0 = 1$ [V · s] is used to make the argument of the logarithm adimensional. Since $\dot{\Lambda} = \lambda^{-1}\dot{\lambda}$, equation (2b) becomes

$$\dot{\Lambda} = \frac{R}{2k_a}x + u - \frac{R(k_b + d)}{2k_a}, \tag{23}$$

where $u = (V/\lambda) = (V/\lambda_0 e^{\lambda})$ [s^{-1}] is the input. Thus, taking x, $\dot{x}$, and Λ as state variables, system (1) is described by

$$\ddot{x} = -\frac{c}{m}\dot{x} - \frac{k}{m}x + \frac{F}{m}, \tag{24a}$$

$$\dot{\Lambda} = \frac{R}{2k_a}x + u - \frac{R(k_b + d)}{2k_a}, \tag{24b}$$

$$F = \frac{\lambda_0^2 e^{2\Lambda}}{4k_a}, \tag{24c}$$

$$u = \frac{V}{\lambda_0 e^{\Lambda}} \leq \frac{V_{max}}{\lambda_0 e^{\Lambda}}, \tag{24d}$$

which consists of two affine dynamical equations, modelling the mechanical and electromagnetic subsystems, and of two non-linear static equations. In order to obtain a piecewise affine model of such system, a piecewise affine approximation of (24c), (24d) as functions of Λ is needed. In particular, equation (24d) is used to enforce the constraint $0 \leq V \leq V_{\max}$ as a piecewise affine constraint on u.

Remark 1: From a mathematical point of view the nonlinear change of coordinate $\Lambda = \ln(\lambda/\lambda_0)$ is valid only in the interval $\lambda \in (0, \infty)$. Constraint (5a) enforces $i \geq 0$, so that we have to discuss only the case $i = 0$. Such an error can be considered as a modelling error, since model (24) is used only for prediction by the MPC controller, and it can be arbitrarily small by leaving Λ unbounded from below. However, in order to maintain the possibility of having a force exactly null, in the piecewise linearization we can impose $F = 0$ for $\Lambda \leq \hat{\Lambda}$, where $\hat{\Lambda}$ is a negative number. As a consequence the modelling error occurs for $0 \leq \lambda \leq \lambda_0 e^{\hat{\Lambda}}$, while for $\lambda = 0$ the approximation error in the force is null.

The piecewise linearization of equations (24c) and (24d) is performed with the approach described in § 4.2.1, where $\chi = \Lambda$. An approximation with four segments for each function is considered,

$$f_j(\Lambda), \quad j = 1, 2, \tag{25}$$

where $j = 1, 2$ indicates the approximation of (24c) and (24d), respectively. Hence, $\ell_j = 4$, $j = 1, 2$, and in total 6 discrete auxiliary variables (16) and 6 continuous auxiliary variables (17) have been introduced. However, because of the additional constraints (19), only 7 combinations of discrete variables are feasible. In particular we have approximated (24c) so that $[\delta_1 = 1] \rightarrow [F = 0]$ and $[\delta_1 = 1] \leftrightarrow [\Lambda \leq \hat{\Lambda}]$, in order to have an exact representation of the force when $i = 0$.

Equations (24a), (24b) and the linearization (25) of equations (24c), (24d) are embedded into an MLD system (21), with three states, three outputs, one input and 12 (6 + 6) auxiliary variables.

6.2 *Simulation of the MPC controller based on the coupled model*

A hybrid MPC controller (22) can be designed, where (22b) is the MLD approximation of (24) computed in § 6.1 and

$$\xi = \begin{bmatrix} x \\ \dot{x} \\ \Lambda \end{bmatrix}.$$

Constraints (3), (4) are enforced as soft constraints, while the input constraint

$$0 \leq V \leq V_{\max}, \tag{26}$$

where $V_{\max} = 350$ V, is enforced as a hard constraint embedded in the MLD model, by exploiting the piecewise affine approximation of (24d).

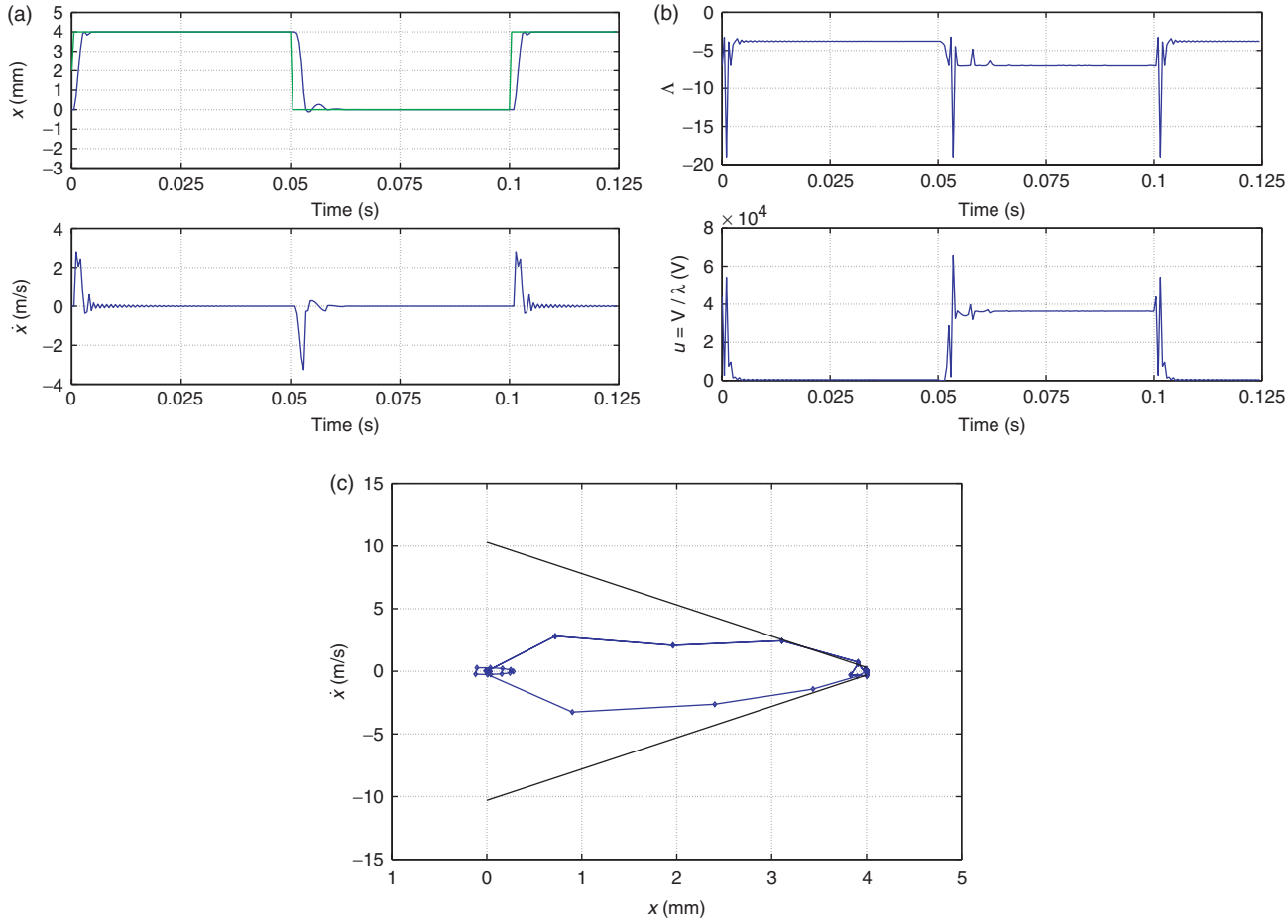

Figure 10. Coupled hybrid model predictive control: (a) trajectories of the mechanical subsystem; (b) trajectories of the electromagnetic subsystem; (c) phase plane of the mechanical subsystem.

The prediction horizon is $N=3$, the cost matrices and the input/output bounds are

$$Q_\xi = Q_N = \begin{bmatrix} 2\cdot 10^{10} & 0 & 0 \\ 0 & 5 & 0 \\ 0 & 0 & 1 \end{bmatrix}, \quad Q_u = 10^{-8},$$

$$y_{\min} = \begin{bmatrix} -4\cdot 10^{-3} \\ -\infty \\ -10.2 \end{bmatrix}, \quad y_{\max} = \begin{bmatrix} 4\cdot 10^{-3} \\ 10.2 \\ +\infty \end{bmatrix},$$

$$u_{\min} = -\infty, \quad u_{\max} = \infty, \quad \rho = 10^{14}.$$

The maximum voltage constraints are embedded into the MLD model. With regards to the third state component, $\Lambda - \Lambda_0$ is weighted in the cost function. By setting $\Lambda_0 = \hat{\Lambda} = -7$, the reference value for the flux $\lambda = \lambda_0 e^{\Lambda}$ is practically zero.

Figure 10 reports the nominal results obtained for the coupled MPC approach when tracking the same reference as in § 5.2. The tracking performance and the mechanical subsystem trajectories are reported in figure 10(a), while figure 10(b) shows the trajectories of the electromagnetic subsystem and of the input signal. The performance is even better than in the ideal case of the decoupled linear/hybrid MPC. This is due to the fact that the voltage constraint is less conservative than the current constraint. The peaks of the input signal u occur when Λ reaches large negative values. This depends on the fact that $V/\lambda_0 e^{\lambda}$ and for $\Lambda \to -\infty$, u is no longer upper-bounded. In figure 10(c) the phase plane behaviour of the mechanical subsystem is illustrated. The landing constraints (4) are slightly violated, as they are treated as soft constraints. Since the state dimension has been increased, there is one additional step of delay in the effects of the input on the position. However, the violation is small, because of the large cost associated to the constraint violation, which forces the system to avoid as much as possible such situations. Table 4 reports the cumulated squared position errors $\sum_k (x(k) - r_x(k))^2$ obtained from the tests in § 4 for

Table 4. Comparison of the decoupled and coupled MPC performances.

MPC controller	Cumulated position error (mm^2)
Decoupled linear MPC	296.0
Decoupled hybrid MPC	237.0
Coupled MPC	149.4

linear and hybrid MPC with inner-loop controller (11) and the one of the coupled MPC controller obtained from the test in this section. Note that the simulation parameters, duration and reference signal $r_x(k)$, in the tests are the same.

The practical advantage of the coupled MPC approach is that the two controllers are fused into a single one, so that the overall system dynamics are optimized, while enforcing constraints also on the voltage. On the other hand, the optimal control problem becomes more complex, so that in our preliminary tests the explicit version of the coupled MPC controller has about 11,000 regions, and therefore much more complex than the linear and hybrid MPC controllers described in the previous sections. Even if it is possible to reduce the controller complexity, for instance, by absorbing small regions (i.e., regions that have a Chebychev radius smaller than a given threshold) into the neighbouring ones, the coupled MPC controller will remain certainly much more complex than the decoupled MPC controllers.

7. Conclusions

We have presented different model predictive control schemes for controlling a magnetically actuated mass-spring-damper system for automotive applications. Two different strategies are based on decoupling the mechanical and electromagnetic subsystems. The resulting MPC controllers optimize only the mechanical subsystem behaviour, while the electromagnetic subsystem is controlled by an inner-loop controller that provides a fast current dynamics. The decoupled MPC controllers have been tested in closed-loop with the nonlinear system, and with the inner-loop controller implemented through feedback linearization. A third MPC approach based on the coupled model of the system has been analysed.

Although the third approach may be more difficult to implement because of its computation complexity, still it provides an assessment of the achievable performance, therefore proving that the first two computationally simpler approaches perform reasonably well but also some significant room for improvement.

An experimental setup is currently under development at the Automatic Control Laboratory of the University of Siena to test the developed algorithms.

Acknowledgements

Work partially supported by the European Commission under the HYCON Network of Excellence, contract number FP6-IST-511368, by Ford Motor Company, and by the Italian Ministry for Education, University and Research (MIUR) under project ''Advanced control methodologies for hybrid dynamical systems''.

References

L. Guzzella and A. Sciarretta, *Vehicle Propulsion Systems Introduction to Modeling and Optimization*, Berlin Heidelberg, Germany: Springer Verlag, 2005.

D. Hrovat, J. Asgari and M. Fodor, ''Automotive mechatronic systems'', in *Mechatronic Systems, Techniques and Applications: Volume 2 – Transportation and Vehicle Systems*, C. Leondes, Ed., Amsterdam: Gordon and Breach Science Publishers, 2000, pp. 1–98.

M. Barron and W. Powers, ''The role of electronic controls for future automotive mechatronic systems'', *IEEE/ASME Transactions on Mechatronics*, 1, pp. 80–88, 1996.

S. Qin and T. Badgwell, ''A survey of industrial model predictive control technology'', *Control Engineering Practice*, 93, pp. 733–764, 2003.

J. Maciejowski, *Predictive Control with Constraints*, Englewood Cliffs, NJ: Prentice Hall, 2002.

E. Camacho and C. Bordons, *Model Predictive Control*, London, UK: Springer-Verlag, 2004.

N. Giorgetti, A. Bemporad, E.H. Tseng and D. Hrovat, ''Hybrid model predictive control application towards optimal semi-active suspension'', *Int. Jour. of Control*, 79, pp. 521–533, 2006a.

N. Giorgetti, G. Ripaccioli, A. Bemporad, I. Kolmanovsky and D. Hrovat, ''Hybrid model predictive control of direct injection stratified charge engines'', *IEEE/ASME Trans. on Mech.*, 11, pp. 499–506, 2006b.

D. Dyntar and L. Guzzella, ''Optimal control for bouncing suppression of CNG injectors'', *ASME J. Dyn. Syst., Measure. Cont.*, 126, pp. 47–45, 2004.

R. Isermann, *Mechatronic systems: Fundamentals*, Berlin: Springer, 2005.

I. Kolmanovsky and E.G. Gilbert 374-375, ''Landing reference governor'', in *Proc. American Contr. Conf.*, Arlington, VA, pp. 374–375, June 2001.

I. Miller, E.G.I. Kolmanovsky, E.G. Gilbert and P. Washabaugh, ''Control of constrained nonlinear systems: a case study'', *IEEE Cont. Syst. Mag.*, 20, pp. 23–33, 2000.

J. Rawlings, ''Tutorial overview of model predictive control'', *IEEE Control Systems Magazine*, 20, pp. 38–52, June 2000.

A. Bemporad, M. Morari, V. Dua and E. Pistikopoulos, ''The explicit linear quadratic regulator for constrained systems'', *Automatica*, 38, pp. 3–20, 2002.

T. Johansen, ''Approximate explicit receding horizon control of constrained nonlinear systems'', *Automatica*, 40, pp. 293–300, 2004.

L. Bleris, P. Vouzis, M. Arnold and M. Kothare, ''A co-processor FPGA platform for the implementation of real-time model predictive control'', in *Proc. American Contr. Conf.*, Minneapolis, MN, pp. 1912–1917, June 2006.

K. Ling, S. Yue and J. Maciejowski, "A FPGA implementation of model predictive control", in *Proc. American Contr. Conf.*, Minneapolis, MN, pp. 1930–1935, June 2006.

S. Boyd and L. Vandenberghe, *Convex Optimization*, New York, USA: Cambridge University Press, 2004.

A. Bemporad, *Hybrid Toolbox – User's Guide*, December 1, 2003, http://www.dii.unisi.it/hybrid/toolbox

E. Sontag, "Nonlinear regulation: the piecewise linear approach", *IEEE Trans. Automatic Control*, 26, pp. 346–358, April 1981.

A. Bemporad and M. Morari, "Control of systems integrating logic, dynamics, and constraints", *Automatica*, 35, pp. 407–427, 1999.

F. Torrisi and A. Bemporad, "HYSDEL — A tool for generating computational hybrid models", *IEEE Trans. Contr. Systems Technology*, 12, pp. 235–249, 2004.